Article

Not peer-reviewed version

In Situ Gelling Behavior and Biopharmaceutical Characterization of Nano-Silver Loaded Poloxamer Matrices Designed for Nasal Drug Delivery

Nadezhda Ivanova *, Neli Ermenlieva, Lora Simeonova, Neli Vilhelmova-Ilieva, Kameliya Bratoeva, Georgi Stoyanov, Velichka Andonova

Posted Date: 23 April 2024

doi: 10.20944/preprints202404.1537.v1

Keywords: silver nanoparticles; chlorhexidine; Kolliphor P407; thermogelation; phase transition; sol-gel transition; protective nasal spray; respiratory infections; prophylaxis; virucidal activity

 doi:10.20944/preprints202404.1537.v1

Article

In Situ Gelling Behavior and Biopharmaceutical Characterization of Nano-Silver Loaded Poloxamer Matrices Designed for Nasal Drug Delivery

Nadezhda Ivanova [1,*], Neli Ermenlieva [2], Lora Simeonova [3], Neli Vilhelmova-Ilieva [3], Kameliya Bratoeva [4], Georgi Stoyanov [5] and Velichka Andonova [1]

[1] Department of Pharmaceutical Technologies, Faculty of Pharmacy, Medical University of Varna, 9000 Varna, Bulgaria; Velichka.Andonova@mu-varna.bg
[2] Department of Microbiology and Virology, Faculty of Medicine, Medical University of Varna, 9000 Varna, Bulgaria.; Neli.Ermenlieva@mu-varna.bg
[3] Department of Virology, Stephan Angeloff Institute of Microbiology, Bulgarian Academy of Sciences, 26 G. Bonchev Str., 1113 Sofia, Bulgaria; losimeonova@gmail.com; nelivili@gmail.com
[4] Department of Physiology and Pathophysiology, Faculty of Medicine, Medical University, "Prof. Dr. Paraskev Stoyanov", 55 Marin Drinov str., Varna, Bulgaria; k_brat@abv.bg
[5] Clinical Pathology, Complex Oncology Center, 9700 Shumen, Bulgaria; georgi.geesh@gmail.com
* Correspondence: Nadezhda.Ivanova@mu-varna.bg

Abstract: A combination of Poloxamer 407 (P407) and hydroxypropyl methylcellulose (HPMC) hydrosols is proposed as an in situ thermo-gelling vehicle for the nasal drug delivery of chlorhexidine-silver nanoparticles conjugates (SN-CX). Varying ratios of P407 and HPMC were applied in the presence and absence of SN-CX in order to optimize the gelation temperature (T_g) to values close to the physiological nasal such (30–34°C). Mechanisms for the observed gelation phenomena were suggested based on viscosimetry, texture analysis, and dynamic light scattering. Tests were carried out for sprayability, washout time, in vitro drug release, ex vivo permeation, and antimicrobial activity. When applied separately, HPMC was found to lower the P407 gelation temperature, whereas SN-CX increased it. However, in the presence of HPMC, SN-CX interfered with the P407 micellar organization in a principally contrasting way, while leading to an even further decrease in T_g. SN-CX-loaded nasal formulation composed of P407 16% and HPMC 0.1% demonstrated a desired gelation at 31.9 °C, good sprayability (52.95% coverage of the anterior nasal cavity), mucoadhesion for 70 min under simulated nasal clearance, expedient release and permeation, and preserved anti-infective activity against seasonal Influenza virus and beta-coronavirus, *Pseudomonas aeruginosa, Klebsiella pneumoniae, Staphylococcus aureus* and other pathogens. Our findings suggest that the current development could be considered a potential formulation of a protective nasal spray against respiratory infections.

Keywords: silver nanoparticles; chlorhexidine; Kolliphor P407; thermogelation; phase transition; sol-gel transition; protective nasal spray; respiratory infections; prophylaxis; virucidal activity

1. Introduction

In situ gelling pharmaceutical formulations find a broad application as drug delivery systems when prolongation of the retention time at the site of administration is required to improve the therapeutic result. Upon reaching the designated biological compartment, these polymeric systems undergo sol-to-gel transition initiated by different stimuli such as changes in the temperature, pH, ionic environment, or else [1-3]. Thereby, they ensure drug immobilization into a highly viscous layer, adherence to the target region, and sustainable effect. The usage of in situ gelling vehicles is highly appropriate in the development of nasal dosage forms for local, systemic or nose-to-brain drug delivery [1,4,5,6].

The protective nasal formulations are a subject of growing interest in this post-COVID-19 pandemic period [7]. Since society's self-awareness of complying with the public health culture principles was provoked, scientists get more and more engaged in developing new, alternative, and

 doi:10.20944/preprints202404.1537.v1

more efficient ways for reducing the spread of infectious respiratory diseases [8]. The protective nasal sprays may exhibit different mechanisms of action but, in general, they concentrate on supporting the natural defense capacity of the nasal mucosa, enhancing the biophysical barrier function of the mucus, and/or exerting microbicidal activity at the site of the pathogen's entry [9]. An effective protective nasal formulation is required to possess good sprayability; to form stable, even, and retentive film on the mucosa; to not harm the nasal cilia; and to preserve the active ingredients' activity by ensuring physical and chemical stability, compatibility, and adequate drug liberation [1,9].

The thermo-sensitive Poloxamer 407 (poly(ethylene oxide)-poly(propylene oxide)-poly(ethylene oxide) triblock copolymer) – P407, was selected as the main constituent in the composition of in situ gelling nasal spray for protection against respiratory infections. The polymer is known for its low toxicity, good tolerability, great chemical inertness, and drug-polymer compatibility [2,10]; because of its amphiphilic nature, P407 self-assembles into micelles which aggregate with the increase in temperature and form a crystal network (solid gel) [11,12]. The gelation temperature (T_g) of P407 solutions depends on the polymer's concentration and the presence of additives such as active pharmaceutical ingredients and excipients [11]; in any case, the gelation of P407 ≥15 w/w% aqueous solutions occurs in a temperature range appropriate for biomedical applications [13,14].

Often, P407 is combined with other polymers in order to improve the formulation's adhesiveness and gel strength (e.g. cellulose derivatives, chitosan, carbomer, poly(vinyl)pyrrolidone) [14,15]. In this study, we focused on hydroxypropyl methylcellulose (HPMC) – a polymer with thermoreversible gelation manifesting at much higher than physiological temperature (>65°C) but with good bioadhesive properties [14,16,17]. It was hypothesized that a P407-HPMC combination could be obtained with an eligible for nasal application adhesive properties, low viscosity and good sprayability at the ambient temperature, and gelation point in the temperature range of the nasal cavity (30-34°C) [4,18].

Ultimately, this study aimed to result in the establishment of a suitable vehicle for the nasal delivery of chlorhexidine-silver nanoparticles conjugates (SN-CX) as an active ingredient. SN-CX were previously synthesized in our laboratories and characterized with explicit antimicrobial properties against Influenza Type A, *Staphylococcus aureus, Escherichia coli*, and *Candida albicans* [19]. Our ongoing research follows the SN-CX activity against these and other respiratory pathogens (seasonal beta-coronavirus, *Pseudomonas aeruginosa,* and *Klebsiella pneumoniae*) when in the composition of the co-polymeric solution and the biopharmaceutical characteristics of so-obtained nasal spray. Although several research papers have reported the inclusion of silver nanoparticles (SN) into P407-based thermogelling vehicles [20-25], the mechanisms by which nano-silver colloids interfere with the P407 micellization and gelation haven't yet been widely explored. We attempted a step-wise investigation of the SN-CX impact on the micellar arrangement and point of solidification of P407 hydrosols and combined P407-HPMC hydrosols.

2. Results and Discussion

2.1. Optimization of the In-Situ Gelling Nasal Composition Based on Viscosimrtry, T_g, Textural, and Colloidal Properties

2.1.1. Viscosimetry

The viscosimetry revealed an increase in viscosity and a sol-gel transition with the rise in temperature up to 45°C for all test formulations; exceptions made the HPMC 0.5% solutions, whose inherent temperature-dependent viscosity was not significantly affected by the presence of SN-CX (within the test temperature range), and the P407 15.5% solutions, combined with HPMC. P407 20% hydrosol was found to undergo gelation at 22.7°C, while P407 20% hydrosol containing conjugates of silver nanoparticles with chlorhexidine (SN-CX), solidified at 26.1°C. Contrariwise, HPMC 0.1%-enriched P407 solutions showed a decrease in T_g as compared to pure P407 solutions with the same concentration. These findings are in accordance with other reports from original studies on the subject [2,14,26,27].

Based on the results from this primary screening, the test formulations were obtained by mixing stock solutions of both hydrosols – P407 20% and HPMC 0.5%, in varying ratios; upon this procedure,

 doi:10.20944/preprints202404.1537.v1

formulations with gradiently dropping P407 and raising HPMC concentrations were yielded. As the proportion of the HPMC hydrosol in the formulation increased, expectedly, gelation was observed at higher temperatures due to the stepwise dilution of the P407 hydrosol [27]. However, an interesting observation was that the presence of SN-CX in the combined solutions (otherwise shown to increase the pure P407 sols gelation point) opposed this tendency and SN-CX-containing P407-HPMC mixtures at all ratios crystallized at lower temperatures as compared to the respective free from SN-CX analogs (Figure 1).

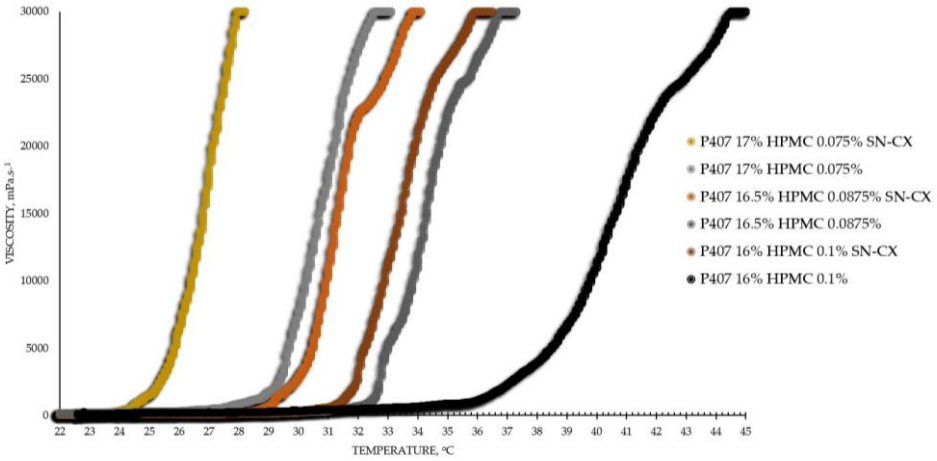

Figure 1. Viscosity-temperature curves of SN-CX-loaded and drug-unloaded P407-HPMC test formulations.

As a practical contribution of this analysis, the formulation P407 16% HPMC 0.1% SN-CX was selected as an appropriate in situ gelling formulation for nasal administration because of its favorable T_g at 31.9°C; the temperature in the nasal cavity is reported to be in the range 30-34°C [4,18]. Furthermore, the formulation in question was characterized with suitable for spaying low viscosity at room temperature (120 mPa.s, Table 1) [4].

Table 1. Viscosity, T_g, DLS analysis, and textural analysis of the test formulations.

Formulation	Viscosity (25°C), mPa.s ±SD	T_g, °C	DLS at 15°C			Texture analysis at 34°C				pH
			Z-average, nm ±SD	Diffusion coefficient, $\mu m^2.s^{-1}$ ±SD	d_{90} ±SD	Span ±SD	Firmness, g ±SD	Adhesiveness, g.s ±SD	Cohesiveness, g.s ±SD	
P407 20%	>29 999	22.7	28.85±2.13	12.79±0.83	4.37±0.53	0.47±0.021	109.33±22.09	23.03±7.26	135.43±29.94	6.5
HPMC 0.5%	4.87±0.09	n.a.	412.07±35.26	0.90±0.05	478.28±51.92	0.52±0.022	n.a.	n.a.	n.a.	n.a.
P407 17% HPMC 0.075%	258.31±14.69	29.2	n.a.	n.a.	n.a.	n.a.	n.a.	n.a.	n.a.	n.a.
P407 16.5% HPMC 0.088%	161.45±13.07	32.3	n.a.	n.a.	n.a.	n.a.	n.a.	n.a.	n.a.	n.a.
P407 16% HPMC 0.1%	130.27±2.84	38.0	170.04±20.77	2.17±0.15	4.38±0.53	0.53±0.026	110.67±10.84	24.97±4.58	119.53±14.29	6.0

 doi:10.20944/preprints202404.1537.v1

P407 15.5% HPMC 0.113%	60.00±0.00	>45	n.a.	n.a.	n.a.	n.a.	n.a.	n.a.	n.a.	n.a.
P407 16%	30.53±3.97	43	n.a.	n.a.	n.a.	n.a.	n.a.	n.a.	n.a.	n.a.
SN-CX	n.a.	n.a.	394.84±42.86	0.93±0.06	344.05±42.02	0.50±0.020	n.a.	n.a.	n.a.	n.a.
P407 20% SN-CX	7 011.64 ±1125.73	26.1	77.12±5.80	4.78±0.27	4.76±0.42	0.67±0.025	100±16.97	20.9±7.50	113.33±17.96	6.0
HPMC 0.5% SN-CX	4.67±0.15	n.a.	864.52±60.39	0.43±0.02	772.28±83.84	0.51±0.020	n.a.	n.a.	n.a.	n.a.
P407 17% HPMC 0.075% SN-CX	1664.15±713.43	25.3	n.a.	n.a.	n.a.	n.a.	n.a.	n.a.	n.a.	n.a.
P407 16.5% HPMC 0.088% SN-CX	147.87±7.83	29.5	n.a.	n.a.	n.a.	n.a.	n.a.	n.a.	n.a.	n.a.
P407 16% HPMC 0.1% SN-CX	120.00±0.00	31.9	655.54±71.16	0.56±0.04	694.93±84.87	0.65±0.029	105.33±5.57	24.83±3.18	115.77±14.14	6.0
P407 15.5% HPMC 0.113% SN-CX	30.00±0.00	>45	n.a.	n.a.	n.a.	n.a.	n.a.	n.a.	n.a.	n.a.

From an analytical point of view, we found that separately SN-CX increased the T_g of P407, and HPMC – decreased it. Still, when applied to a combined P407-HPMC solution, the colloidal particles further potentiated the gelation and decreased the T_g. To investigate these phenomena, a DLS analysis was performed and a mechanism for the occurrence of this controversy was proposed (Figures 2 and 3).

 doi:10.20944/preprints202404.1537.v1

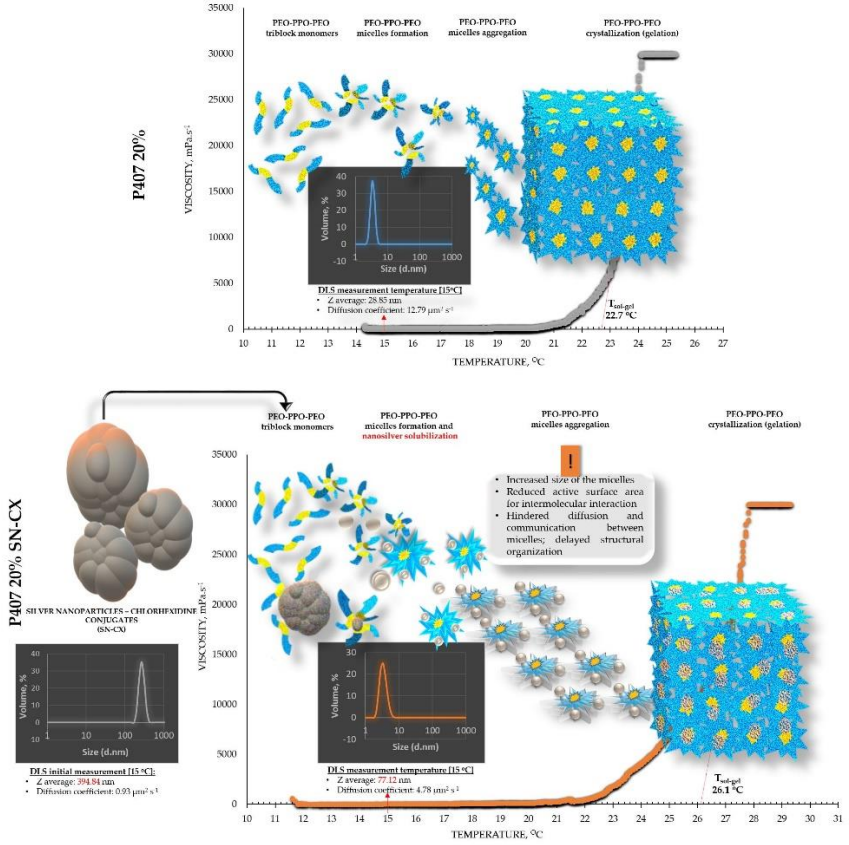

Figure 2. Speculative illustration of the mechanism of gelation of P407 sols and SN-CX-loaded P407 sols.

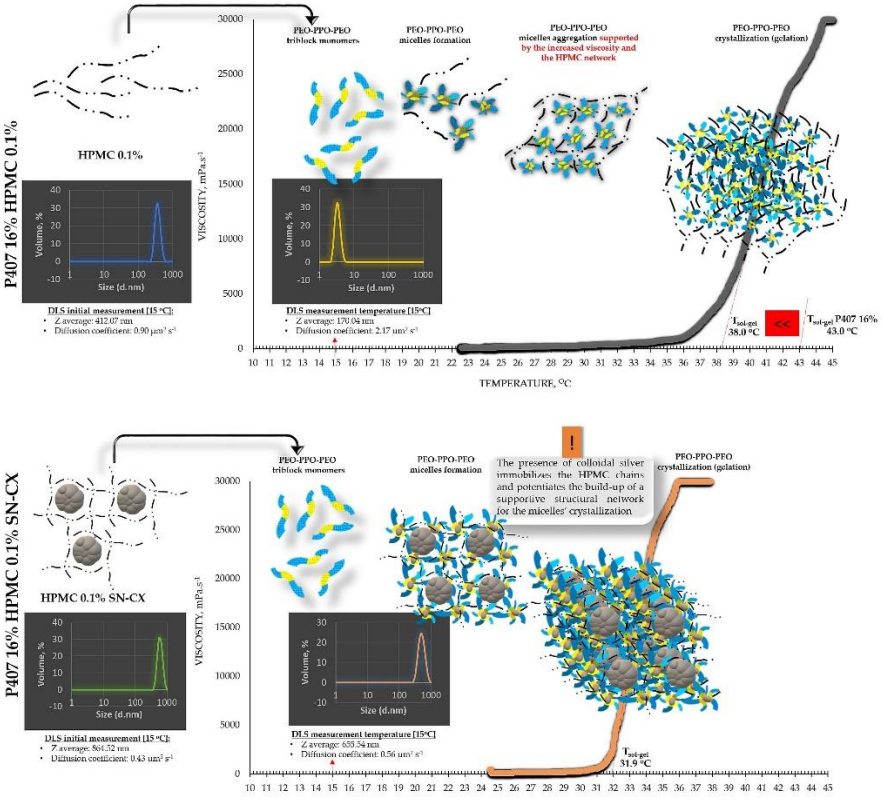

Figure 3. Speculative illustration of the mechanism of gelation of P407-HPMC combined sols and SN-CX-loaded P407-HPMC combined sols.

 doi:10.20944/preprints202404.1537.v1

2.1.2. Dynamic Light Scattering (DLS)

DLS analysis was carried out for all single components and mixtures of interest. A decision was made to perform the tests at a temperature low enough to ensure a sol state of all samples – 15°C. The results from the front angle (12.78°) scans were considered as they demonstrated eligibility for comparative purposes for all materials. Under these conditions, the hydrodynamic diameter (d_H, Z-average, nm) of the colloidal SN-CX conjugates was found to be 394.84±42.86 nm; visibly, d_H drastically decreased, when the nanoparticles were introduced into the P407 20% solution (77.12±5.80 nm), thus suggesting micelle-assisted solubilization and localization amongst the hydrophilic poloxamer (P407) regions [28,29]. On the contrary, when the same concentration of SN-CX was included in a HPMC 0.5% solution, a more than two-fold increase in d_H (864.52±60.39 nm) revealed adsorption of the negatively charged polymer (-) onto the positive (+) colloidal surface of SN-CX (ζ = +44.59 [19]) [30]. Indeed, the visual appearance of both SN-CX-carrying solutions was compliant with this result since P407 20% SN-CX appeared as a fully transparent yellow solution, while HPMC 0.5% SN-CX possessed an orange-brown color and a slight opalescence. When SN-CX was placed in a combined solution of P407 16%-HPMC 0.1%, the obtained d_H values of 655.54±71.16 nm eloquently testified that the silver nanoparticles' solubilization is limited by the HPMC shield on the particles' surface and their respective enlargement.

The colloids' diffusion coefficients were derived because of their straight relation to the particles' mobility, interaction, and ability to assemble into organized structures (determining the point of gelation); they were all found to correspond well with the average hydrodynamic size in the system. Because of the complexity and heterogeneity of the colloidal mixtures, d_{90} and span values were also considered; the first parameter indicates the size limit within the predominant part of 90% of the sample, while the latter is a measure of the size distribution within the sample. All data from the DLS analysis is presented in Table 1.

2.1.3. Texture Analysis

HPMC was chosen as a second polymeric ingredient in the thermo-gelling nasal vehicle in order to improve the formulation's adhesiveness and gel strength. When P407 20% and HPMC 0.5% solutions were mixed in an 80:20 ratio (in order to form a vehicle with an appropriate gelation point – 31.9°C), a final concentration of P407 16% HPMC 0.1% was obtained. Textural analysis of P407 20% and P407 16% HPMC 0.1% in the presence and absence of SN-CX was performed. Although the addition of HPMC solution decreased the P407 concertation from 20% to 16%, it was proven to not only retain but also slightly increase the firmness and adhesiveness of the formed gel at 34°C, while reducing the cohesiveness. The same observation was made in the presence of SN-CX, except for the cohesiveness; the latter was relatively lower for SN-CX-enriched gels as compared to the drug-unloaded gels and was not significantly different for both P407 20% SN-CX and P407 16% HPMC 0.1 % SN-CX formulations. This result is likely due to the hypothesized conformational changes in the system caused by the integration of silver nanoparticles in the hydrophilic micellar regions and corresponds with the observed effect of SN-CX on P407 gelation. In addition, the presence of SN-CX weakly reduced the firmness and adhesiveness of both test gels as well, as compared to the drug-unloaded analogs (Figure 4, Table 1).

Preprints.org (www.preprints.org) | NOT PEER-REVIEWED | Posted: 23 April 2024 doi:10.20944/preprints202404.1537.v1

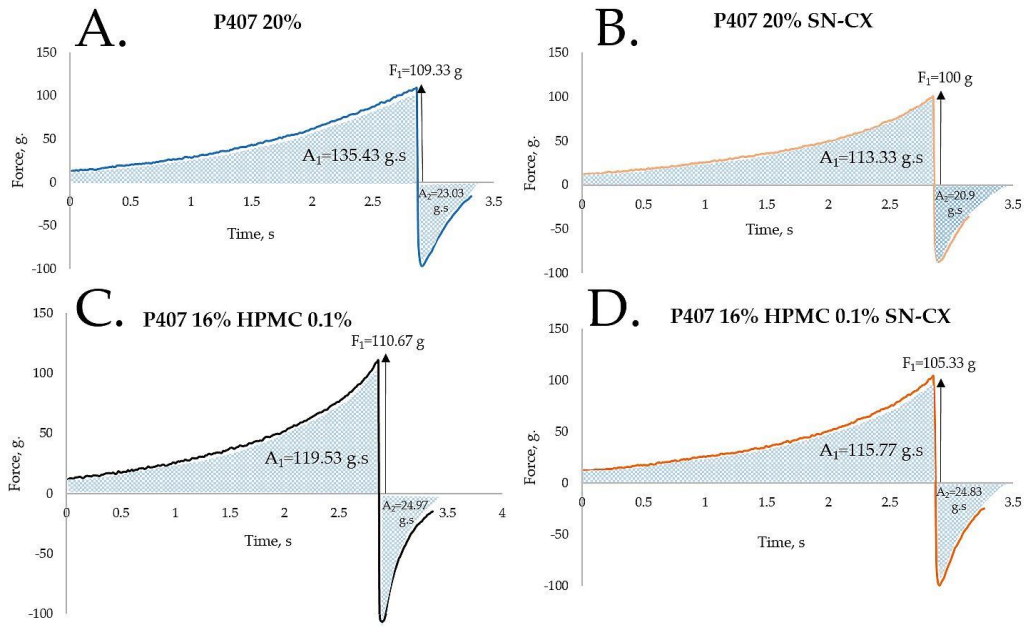

Figure 4. Texture analysis of (a) P407 20% hydrogel, (b) P407 20% SN-CX hydrogel, (c) P407 16% HPMC 0.1% hydrogel, and (d) P407 16% HPMC 0.1% SN-CX hydrogel at 34°C.

2.2. Sprayability

The proposed nasal formulation – P407 16% HPMC 0.1% SN-CX was tested against a water solution in order to follow the influence of the polymeric mixture on the solution's ability to be sprayed and spread along the anterior nasal cavity. Both, the test and the control samples were colored in advance with a water-soluble red dye so that the sprayed-on material could be color-analyzed. The loss of sprayability due to an increased viscosity of the test formulation was calculated to be only 12.55% as compared to the performance of pure water injected with the same spraying device. This result was achieved after three-in-a-row injections of the formulations in the nasal cavity model. We should acknowledge that the difference in the covered area between the test and control spray was greater and not as satisfactory when one or two in a row injections were applied. An advantage of the polymeric solution was the better retention on site and the lack of leakage to the throat. It should be noted that the proposed methodology did not allow simulation and consideration of the airflow forces arising upon the recommended sharp inhale while spraying in the nose. We reckon that this method of sprayability testing could be applied as an easy and affordable to reproduce alternative technique in the process of pharmaceutical development; this should be only done when better simulation models (such as 3D printed nasal casts or software-assisted models for digital simulations [31,32]) are not available. The results from the sprayability test are presented in Figure 5. The color analysis was performed as shown in Figure 6.

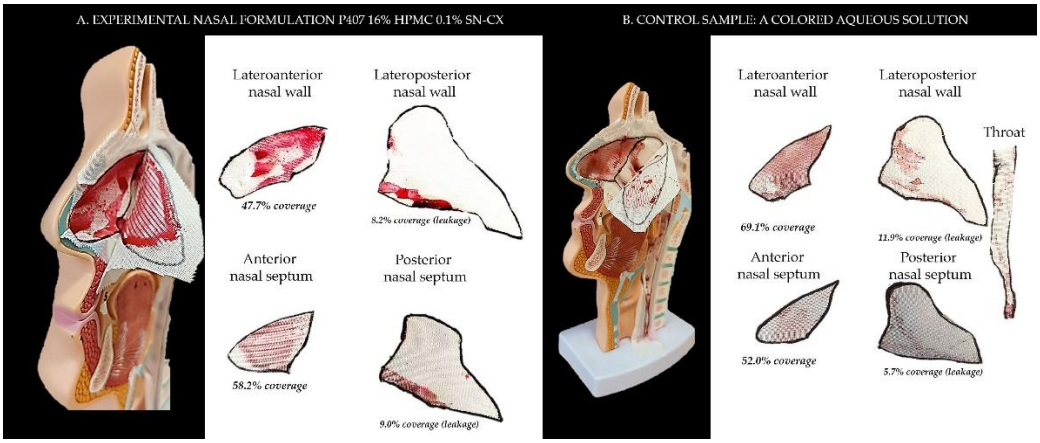

 doi:10.20944/preprints202404.1537.v1

Figure 5. Sprayability of (a) P407 16% HPMC 0.1% SN-CX against (b) colored water solution, assessed by the area covered (%) in a simulated nasal cavity model: the role of the delivery vehicle .

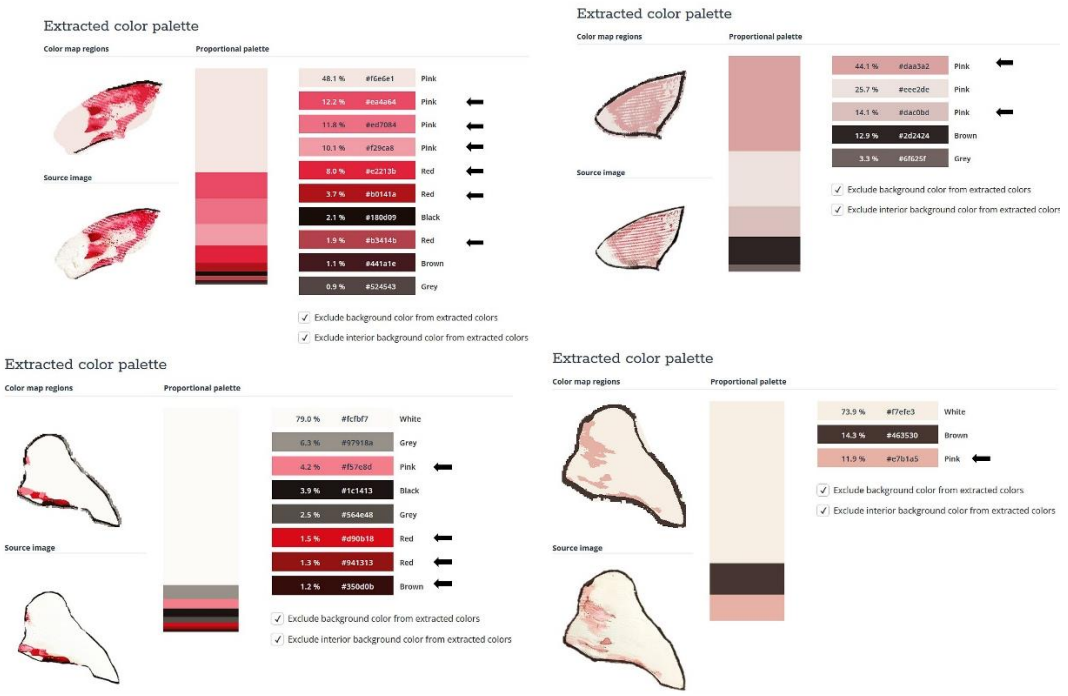

Figure 6. Color analysis of sprayed and dried artificial tissues performed online on https://labs.tineye.com.

2.3. Washout Time/Mucosal Retention

In this study, we aimed to emphasize the role of HPMC in the composition and compared the mucosal retention of the optimized nasal formulation – P407 16% HPMC 0.1% SN-CX, with the one of P407 20% SN-CX. This was done upon vertical positioning and fixation of the mucosal tissue and under simulated nasal flow. The time to complete washout was recognized with the aid of methylene blue dye added to the samples in advance. For P407 20% SN-CX, it was registered to be approximately 40 min, and for P407 16% HPMC 0.1% SN-CX – 70 min. The photographs in Figure 7 demonstrate the beginning and end point of the experiment and the washout zone determined by the path of the drops.

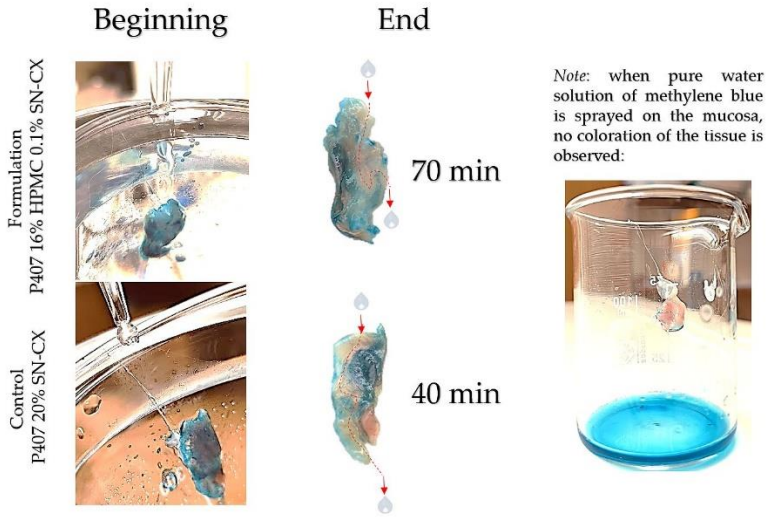

 doi:10.20944/preprints202404.1537.v1

Figure 7. Washout zone and retention time of test formulation P407 16% HPMC 0.1% SN-CX against control formulation P407 20% SN-CX: the role of the mucoadhesive HPMC polymer.

Since warm water (34°C) was used as a washing fluid in this test and a flow rate comparable to the average physiological nasal secretion debit was maintained (2000 ml per day) [33], we may reckon that the obtained results relate to an extreme case scenario in which the nasal mucus would acquire a viscosity comparable to water under high shear rates typical for sniffing, sneezing, etc. [34].

2.4. In Vitro Drug Release and Ex Vivo Mucosal Permeation

The drug liberation from P407 16% HPMC 0.1% SN-CX and the actual permeation through nasal mucosa did not show any notable differences of practical significance. Indeed, the ex vivo study allowed a higher concentration of silver ions in the receptor compartment as compared to the quantity released through the artificial dialysis membrane. Most importantly, neither of the membranes allowed permeation of silver nanoparticles; likely due to the complex structure and the larger hydrodynamic diameter of the nanoparticles in the composition, SN-CX were still undetectable in the receptor media by UV-Vis spectrophotometry after the 3rd hour of the experiments. Despite the broad-spectrum activity, the lack of biodegradation of silver nanoparticles is considered the main disadvantage of this type of nanotechnology [35]. Hence, this result fits a desired case scenario – formulated SN-CX release their active components, i.e. chlorhexidine and silver ions, by dissociation and degradation, respectively, but do not penetrate the mucosa and do not set a prerequisite for cumulation and absorption into the bloodstream (Figure 8).

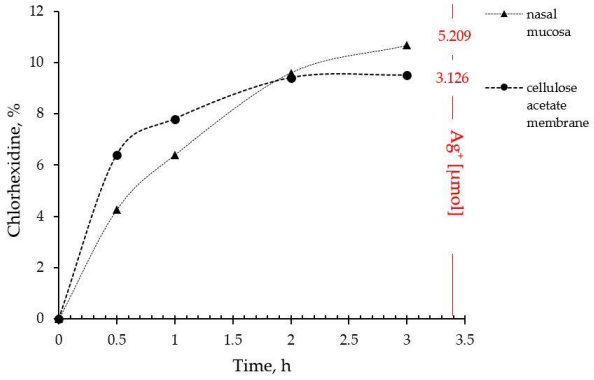

Figure 8. Drug liberation and mucosal permeation from P407 16% HPMC 0.1% SN-CX formulation.

2.5. Antimicrobial Activity

2.5.1. Antibacterial and Antifungal Activity

The SN-CX conjugates were previously proven with antimicrobial activity against *S. aureus*, *C. albicans*, and *E. coli*, and minimal bactericidal/ fungicidal concentrations were found at 28.6 μg.ml^{-1}, 28.6 μg.ml^{-1}, and 14.3 μg.ml^{-1}, respectively (these values relate to the total active concentration of silver nanoparticles plus the equivalent concentration of chlorhexidine linked) [19]. These results were taken into consideration when choosing the active concentration in the nasal formulation (57.19 μg.ml^{-1}). Herein, the antimicrobial potency of SN-CX was assessed within the polymeric solution and compared with the activity of the non-formulated SN-CX colloid. To the test pathogens were added *Pseudomonas aeruginosa* and *Klebsiella pneumoniae* because of their high relevance to respiratory infections and complications [36,37]. Judging by the zones of inhibition on Mueller-Hinton agar, P407 16% HPMC 0.1% SN-CX demonstrated the strongest antimicrobial activity against *C. albicans* (d=21 mm), followed by *K. pneumoniae* (d=20 mm), *S. aureus* (d=17 mm), *P. aeruginosa* (d=14 mm), and *E. coli* (d=12 mm). The zones of inhibition obtained with the pure SN-CX solution at the same concentration were found to be either the same or not more than 2 mm wider as compared to the ones achieved with the SN-CX-loaded nasal formulation (Figure 9, Table 2). Such a slightly decreased effect is

 doi:10.20944/preprints202404.1537.v1

expected upon the application of viscous dosage forms due to a retarded drug release and diffusion [38].

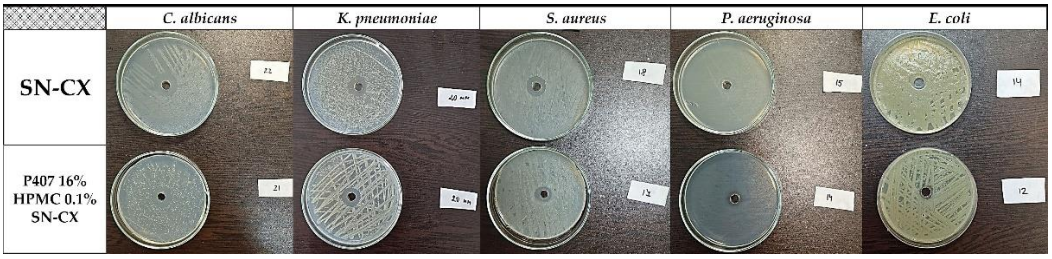

Figure 9. Inhibitory zones of P407 16% HPMC 0.1% SN-CX and SN-CX in seeds of *P. aeruginosa*, *K. pneumoniae*, *S. aureus*, *C. albicans*, and *E. coli* .

Table 2. Inhibitory zones of P407 16% HPMC 0.1% SN-CX and SN-CX in seeds of *P. aeruginosa*, *K. pneumoniae*, *S. aureus*, *C. albicans*, and *E. coli* .

Pathogen	P407 16% HPMC 0.1% SN-CX, mm	SN-CX, mm
C. albicans	21	22
K. pneumoniae	20	20
S. aureus	17	18
P. aeruginosa	14	15
E. coli	12	14

2.5.2. Antiviral and Virucidal Activity

In order to be able to claim that the effect of the test sample on the cell monolayer during the antiviral experiments is due to the viral replication, but not to the cytotoxicity, its cytotoxicity against the cell lines was previously determined. When examining the toxicity of P407 16% HPMC 0.1% SN-CX against the HCT-8 cell line over a period of 120 hours (the time required to determine the antiviral effect in the HCov-OC-43 strain) it was found that the test sample was significantly more cytotoxic compared to the reference substance Remdesivir (REM) used (Table 3).

Table 3. Cytotoxicity of the test sample P407 16% HPMC 0.1% SN-CX against HCT-8 cell line.

Compound	**HCT-8 cell line**	
	CC_{50}[a] Mean ± SD[b] [μg.ml^{-1}]	**MTC[c] [μg.ml^{-1}]**
P407 16% HPMC 0.1% SN-CX	47.5[d] ± 2.8	9.2[d]
REM	2500.0 ± 4.3	1000.0

[a] CC_{50} — cytotoxic concentrations 50%; [b] SD — standard deviation; [c] MTC — maximum tolerable concentration; [d] total active concentration silver nanoparticles plus the equivalent concentration of chlorhexidine.

Regarding cytotoxicity evaluation in MDCK cells, P407 16% HPMC 0.1% SN-CX showed considerably higher toxicity than the reference oseltamivir (OS) 450 μg.ml^{-1}. These data are in accordance with our previous report on SN-CX toxicity, although, herein, in the polymeric milieu, the toxicity against MDCK cells slightly decreases (Table 4) [19].

Table 4. Cytotoxicity of the test sample P407 16% HPMC 0.1% SN-CX against MDCK cell line.

Compound	**MDCK cell line**	
	CC_{50}[a] Mean ± SD[b] [μg.ml^{-1}]	**MTC[c] [μg.ml^{-1}]**
P407 16% HPMC 0.1% SN-CX	4.68[d] ± 2.8	3.0[d]
SN-CX [19]	4.20[d]± 0.6[19]	-
OS	450.0 ± 1.3	360.0

 doi:10.20944/preprints202404.1537.v1

[a] CC_{50} — cytotoxic concentrations 50%; [b] SD — standard deviation; [c] MTC — maximum tolerable concentration; [d] total active concentration of silver nanoparticles plus the equivalent concentration of chlorhexidine bound.

When determining the effect on the replication of HCov-OC-43 and IAV A/Panama/07/99 (H3N2), it was found that P407 16% HPMC 0.1% SN-CX, like pure SN-CX, had no effect on this stage of viral reproduction compared to REM (IC_{50} = 12.5 ± 0.9 μg.ml^{-1}; selectivity index (SI) = 200.0) and OS (IC_{50} = 1.8 μg.ml^{-1}; SI = 250).

The virucidal effect (effect on the viability of extracellular virion particles of corona and influenza virus) of P407 16% HPMC 0.1% SN-CX at its MTC was also investigated. It was found that in the first two incubation time intervals (15 and 30 min) the effect was low and comparable for both viruses (up to 1 Δlg). It slightly increased with the extension of the exposure time and at 60 min, the viability of HCov-OC-43 and influenza virions was reduced by Δlg = 1.5 and Δlg = 1.25, respectively (Tables 5 and 6).

Table 5. Virucidal activity against coronavirus virions strain HCoV-OC-43.

Compound	Δlg			
	15 min	30 min	45 min	60 min
P407 16% HPMC 0.1% SN-CX	0.25	0.75	1.25	1.50
Ethanol 70%	5.0	5.0	5.0	5.0

Table 6. Virucidal activity against influenza virus virions strain A/Panama/07/99 (H3N2).

Compound	Δlg			
	15 min	30 min	45 min	60 min
P407 16% HPMC 0.1% SN-CX	0.25	0.50	1.00	1.25
SN-CX [19]	0	0	0.33	0.33
Ethanol 70%	4.0	4.0	4.0	4.0

The registered virucidal effect against corona and influenza virus is present but weak (compared to standard ethanol 70%) due to the very low MTC of the formulation on HCT-8 and MDCK cell lines. The latter limits drastically the active concentrations to be applied and tested. Still, the obtained results show an increase in the virucidal potency of the nasal formulation in comparison to non-formulated SN-CX [19].

3. Conclusions

An in situ gelling vehicle composed of Poloxamer 407 and hydroxypropyl methylcellulose for the nasal drug delivery of silver nanoparticles-chlorhexidine conjugates (SN-CX) was developed and the effects of this active complex on the formulation's thermogelling and mechanical properties were investigated. A DLS-based analysis allowed us to propose a mechanism for the arising phenomena, which namely were: 1. SN-CX's undergo solubilization in the Poloxamer sols and suppress the micellar crystallization which leads to an increase in the gelation temperature; 2. HPMC potentiates the P407 gelation and their mixture acquire lower gelation temperature compared to only P407-containing sols with corresponding concentrations; 3. When SN-CX and HPMC are both present in the composition of the P407 hydrosols, an additional potentiation of the gelation of P407 is observed and thus even lower gelation temperatures are registered. This interesting finding could be explained by the SN-CX's significantly enlarged hydrodynamic size when HPMC adsorbs on their surface and the subsequent lack of micellar solubilization. Because of these findings, we hypothesized that instead of acting as a conformational obstacle for the micelles' organization, SN-CX's structurally support the HPMC-mediated intermolecular communication within the P407-HPMC solutions.

Within the scope of this study, we propose two original methodologies – for comparative sprayability assessment and comparative mucosal retention time assessment. Both methodologies are

 doi:10.20944/preprints202404.1537.v1

easily reproducible and do not require specific and expensive equipment. Therefore, we consider they could be used as accessible alternatives in the stages of preliminary nasal dosage forms development.

The optimized drug-loaded P407 16% HPMC 0.1% SN-CX test nasal formulation possessed several desirable qualities for its designation: a gelation temperature at 31.9°C; a better adhesiveness and mucosal retention as compared to P407 compositions without HPMC; a good sprayability ensuring a 52.95% coverage of the anterior nasal cavity; an effective Ag^+ and chlorhexidine release and mucosal permeation to which we devote the established antimicrobial activity against *Pseudomonas aeruginosa, Klebsiella pneumoniae, Staphylococcus aureus, Escherichia coli,* and *Candida albicans* and the weak but present after the 45th minute of contact virucidal effect on influenza and coronavirus virions. According to this study, the proposed formulation has shown eligibility for in-situ gelling protective nasal spray on all regarded aspects. As a prospect, an improvement might be sought in terms of lower colloidal size and even less pronounced shielding effect on the antiviral activity.

4. Materials and Methods

4.1. Materials

Silver nitrate at >99.9%, sodium hydroxide pellets at >98%, and ammonium thiocyanate at >98% were purchased from Thermo Fisher Scientific, Oxford, UK. Chlorhexidine diacetate salt hydrate at ≥ 98%, Mw 625.55 g/mol, was supplied from Sigma Aldrich, Burlington, MA, USA; Kolliphor® P407, hydroxypropyl methylcellulose (HPMC) (80-120 cps), and Ammonium iron(III) sulfate dodecahydrate – from Sigma-Aldrich, St. Louis, MO, USA; all organic solvents were purchased from Sigma-Aldrich (USA) and were of analytical grade.

4.2. Silver Nanoparticles-Chlorhexidine Conjugates (SN-CX)

Silver nanoparticles were synthesized by reduction of $AgNO_3$ with green tea phenolic extract and conjugated with chlorhexidine diacetate (CX) following an already established procedure [19,37]. The obtained colloidal solutions were purified by a dialysis method and standardized with a concentration of 700 $\mu g.ml^{-1}$ nano-silver and 1130 $\mu g.ml^{-1}$ conjugated CX [19]. The total active concentration of the stock SN-CX solution was considered the sum of SN and CX – 1830 $\mu g.ml^{-1}$. SN-CX samples were stored at room temperature under light protection and used within a safe period of 7 days [39].

4.3. Preparation of In Situ Gelling Test Formulations

A stock solution of P407 20% was prepared by dispersing the polymer in purified water under static conditions, keeping the so-obtained mixture in a refrigerator for at least 24 h, and gentle homogenization thereafter. Where needed, P407 16% solution was prepared from P407 20% stock solution by proper dilution.

A stock solution of HPMC 0.5% was prepared by dispersing the polymer in preheated purified water at 80°C under continuous stirring, keeping the so-obtained mixture in a refrigerator for at least 24 h, and homogenization thereafter.

Stock solutions of SN-CX-enriched hydrosols with a concentration of 57.19 $\mu g.ml^{-1}$ were prepared by the addition of SN-CX stock solution (3.13% w/w) to previously obtained with a re-calculated quantity of purified water hydrosols of P407 or HPMC so that the final polymeric concentration would be the same as for the drug-unloaded hydrosols – 20% for P407 and 0.5% for HPMC, respectively.

All polymeric stock solutions were stored in a refrigerator before their use. The drug-unloaded test formulations were obtained by mixing stock solutions of P407 20% and HPMC 0.5% in varying ratios – 90:10, 85:15, 80:20, and 75:25. SN-CX-loaded test formulations were obtained likewise by using SN-CX-enriched P407 20% and HPMC 0.5% stock hydrosols.

4.4. pH Measurement

 doi:10.20944/preprints202404.1537.v1

The pH of the test formulations was measured with the aid of Filtres Fioroni pH indicator paper with a pH measurement range of 5.0-9.0.

4.5. Viscosimetry

Viscosity analysis of the test formulations was performed on IKA® Rotavisc lo-vi, IKA®-Werke GmbH & Co. KG, Germany. Spindle № 4 (SP-4) was used at a rotation speed of 20 rpm determining a viscosity range detection up to 30 000 mPa.s. The test samples were introduced in a large volume of 500 ml. The temperature was controlled with the aid of an external water bath and the change in viscosity as a function of the actual sample's temperature was plotted. Values were registered up to 45°C. The obtained data was processed using Microsoft Excel® and the gelation temperature was determined by the trend line passing the ascending region of the curve at minimum R^2=0.95 (the tangential), as shown in the example in Figure 10.

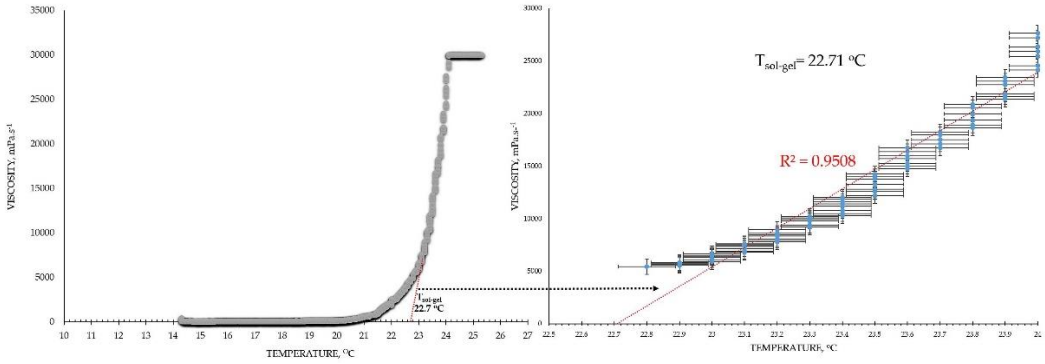

Figure 10. Mathematical extrapolation of the gelation temperature (T_g) based on the gelation curve's tangential [40-42].

Exception from this methodology made the viscosimetry of HPMC 0.5% solutions because of their significantly lower viscosity and lack of sol-gel transition in the investigated temperature interval. They were assessed with the aid of spindle SP-1 at 50 rpm which allowed the best obtainable sensitivity in the expected low viscosity range.

The viscosity at 25°C was calculated for all test formulations as an average of all viscosity values received in the temperature interval between 24.5-25.5°C during the measurements.

4.6. Texture Analysis

The samples of interest were previously filled in appropriate for the test containers and tempered at 34°C in a climatic chamber, Climatest CH 150, ArgoLab, Italy, for at least an hour. A Belle texture analyzer (Agrosta Overseas, Serqueux, France), equipped with a conical probe (40 mm in diameter), was used to measure the mechanical properties of the obtained gels. The selected pretest and test speeds were 3 mm/s, and the insertion depth was 5 cm [43]. All measurements were performed in triplicate. The graphs were built based on the average values.

4.7. Dynamic Light Scattering (DLS)

Multi-angle dynamic light scattering (MADLS) was carried out on a Zetasizer Ultra Red (λ = 632.8 nm) (Malvern Panalytical Ltd., Malvern, UK) at 15 °C. Data was processed and obtained with the aid of the ZS XPLORER 3.2.0.84 software. Parameters such as average hydrodynamic diameter (d_H, Z-average), diffusion coefficient, d_{90}, and span were obtained. All measurements were repeated in triplicate.

4.8. Sprayability

The experimental setting for sprayability testing was built with the aid of a real-sized plastic 3D nasal cavity anatomical model. The surface from the inside was covered with a white synthetic silk surgical tape to allow retention and visibility of the sprayed formulation and removal of the tissue

 doi:10.20944/preprints202404.1537.v1

thereafter; the same material was applied as an improvised nasal septum. The four main zones of the nasal cavity, i.e. lateroanterior nasal wall, lateroposterior nasal wall, anterior septum, and posterior septum, were outlined with a black permanent marker. The spraying device was inserted in the nostril and the angles of spraying were determined thereof (Figure 11). The sprayability of the test nasal formulation was assessed against pure water solution; both, the test and the control solutions were colored with a water-soluble red dye in advance so that a color analysis could be performed for estimation of the covered area. Each solution was sprayed thrice by using the same spraying device. At least an hour before spraying and right after spraying the prepared nasal cavity model was kept at 34°C in a climatic chamber, Climatest CH 150, ArgoLab, Italy. The artificial lining was removed after drying up the sprayed material, cut along the contours, and taped on a blank paper sheet in order for contrast photographs to be taken and color-analyzed. The pictures were taken with a realme 11 Pro+ 32MP camera without magnification. The color analysis was done with the aid of the online color extraction platform of TinEye https://labs.tineye.com/color/. The ability of the formulation to be sprayed was evaluated by the percentage covered area. The loss of sprayability of the test formulation due to the increased viscosity was calculated as follows:

$$\frac{\textbf{Coverage of the lateroanterior nasal wall, \% (Test)} + \textbf{\% Coverage of the anterior nasal septum, \% (Test)}}{\textbf{Coverage of the lateroanterior nasal wall, \% (Control)} + \textbf{\% Coverage of the anterior nasal septum, \% (Control)}} \cdot \mathbf{100} \quad (1)$$

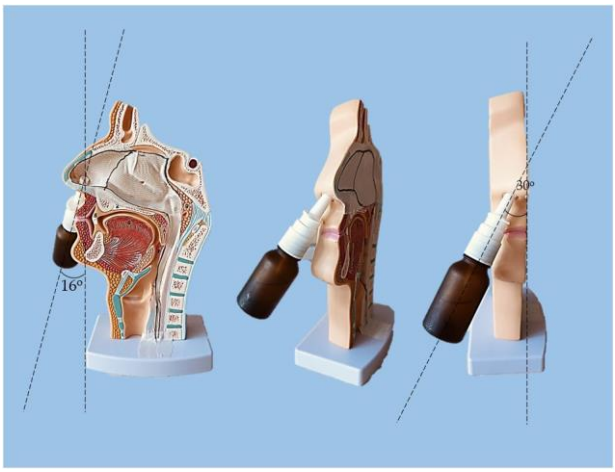

Figure 11. Experimental setting for sprayability testing**.**

4.9. Isolation of Nasal Mucosa Explants

The method for nasal mucosa preparation was selected according to Wadell's et al. methodology [44]. The tissues were obtained from the porcine snout of a pig weighing 80-90 kg and aged 7-8 months in a certified slaughterhouse (Varna, Bulgaria). The snout was opened by pathologists using forceps and a scalpel, and the pieces of nasal mucosa were isolated from the cavity mucosa and placed on ice during transport to the laboratory. Within 60 min of removal, pieces of nasal mucosa were carefully cut with a scalpel of appropriate size for the mucosal retention test and the ex vivo permeation test.

4.10. Determination of Mucosal Retention Time/Washout Time

The experimental setting for mucosal retention time was based on vertical fixation of the mucosal explants, spraying of the test formulations, initiation of simulated nasal flow, and detection of the time required for the appearance of a washed-out zone (Figure 12). Subjects to this test were P407-HPMC drug-loaded optimized formulation and HPMC-free equivalent formulation. Both test samples were colored with methylene blue before spraying on the mucosa. A pure water solution of methylene blue was used as a negative control in order to establish the compound's lack of coloring potential when not in the composition of a viscous and mucoadhesive form. Nasal mucosa explants with an approximate size of 1 x 2 cm were fixated to the upper inner side of an empty beaker glass with the aid of silicone glue. The tissue's temperature was adjusted to 34°C by ensuring tight contact

 doi:10.20944/preprints202404.1537.v1

with an external water bath as shown in Figure 12. So prepared, the setting was allowed to condition for an hour before performing the experiment. A single spray of each formulation was applied to the mucosal explants. A simulation of a nasal flow was initialized by using warm water (34°C)-loaded burettes positioned right above the medial axis of the sprayed mucosal pieces. A flow rate of 1.4 $ml.min^{-1}$ (30 drops per minute) resembling the physiological nasal secretion debit (2000 ml per day) was set [33]. The time required for the appearance of a clear washed-out zone was recorded. The mucosal explants were gently dried with the aid of a filter paper at the end of the experiment and photographs were taken (realme 11 Pro+ 32MP camera without magnification).

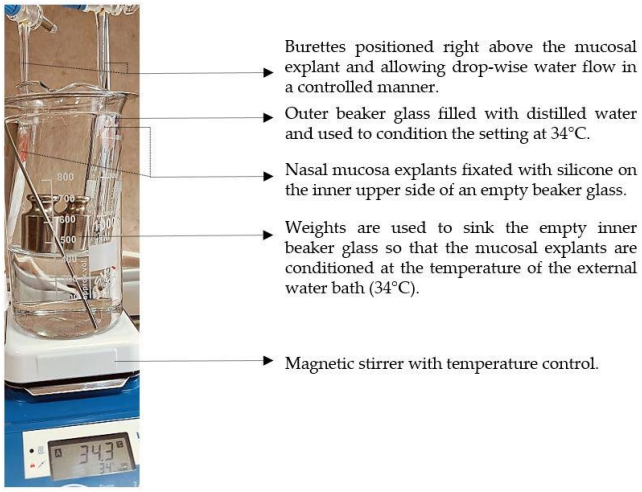

Figure 12. Experimental setting for mucosal retention time testing**.**

4.11. In Vitro Drug Release

A drug release study was carried out on Franz diffusion cell through Spectra/Por® cellulose membrane (MWCO: 12-14 kDa). The cell possessed an exposed membrane surface area of 0.98 cm^2 and a receptor volume of 8 ml. The receptor compartment was filled almost to the top with distilled water and the cell was conditioned at 34 ± 0.5 °C with a circulating thermostatic bath. 0.83 g test hydrosol (corresponding to 1.0 ml formulation at 25 °C) was introduced in the donor compartment and the receptor volume was adjusted to the top. A stirring rate of 1000 rpm was set. A sample of 0.5 ml was withdrawn on 0.5, 1, 2, and 3 h from the receptor media for quantification of SN-CX and CX. UV-Vis spectrophotometric analysis (at λ=439 nm for SN-CX and λ=231 nm for CX [19]) was applied for the purpose and a standard curve calculation was used. The analyzed sample was returned to the receptor compartment and if an adjustment of the volume to the top was needed, distilled water was used. At the end of the experiment titrimetric assay of silver ions (Ag+) was performed by using an adjusted pharmacopoeial method with ferric ammonium sulfate 100 $mg.ml^{-1}$ as indicator and ammonium thiocyanate 0.01 mM as titrant [45].

4.12. Ex Vivo Drug Permeation

An ex vivo permeation study was performed on Franz diffusion cell following the same procedure as described for the in vitro drug release study by using nasal mucosa explant as a membrane. The mucosal tissue was positioned in the cell with the aid of a fixation ring as shown in Figure 13. The mucosal integrity was checked before starting the experiment with a bubble test.

 doi:10.20944/preprints202404.1537.v1

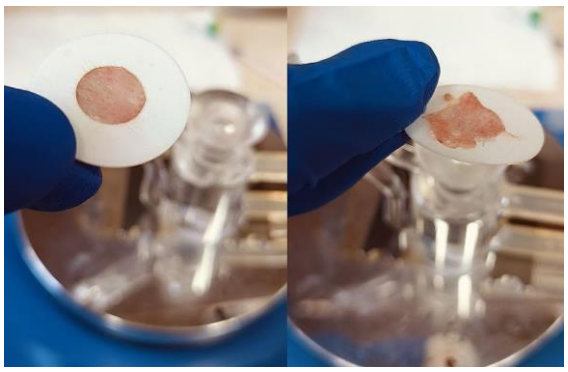

Figure 13. Fixation of the nasal mucosa for the ex vivo permeation study.

4.13. Antimicrobial Activity

4.13.1. Antibacterial and Antifungal Activity

A cup-plate technique was applied for evaluation of the antimicrobial activity of SN-CX and SN-CX-loaded test nasal formulation against *Escherichia coli* ATCC 25922, *Staphylococcus aureus* ATCC 25923, *Candida albicans* ATCC 10231, *Pseudomonas aeruginosa* ATCC 10145, and *Klebsiella pneumoniae* ATCC 10031 (MicroSwabs, Ridacom, Bulgaria). Dense seeds of 0.5 MF standardized microbial suspensions were made on Mueller–Hinton agar (HiMedia®, Ridacom, Bulgaria). After drying, using a sterile borer, a 7 mm-wide well was carved in the center of each Petri's agar and filled with 100 µL of the test formulation. The Petri dishes were incubated aerobically for 24 hours at 37°C for the bacterial cultures and 48 hours at 35°C for *C. albicans*; after that, the emerged inhibition zones were measured in diameter.

4.13.2. Cytotoxicity, Antiviral and Virucidal Activity

Cells

Human colon carcinoma (HCT-8) cells were purchased from the American Type Culture Collection (ATCC). Permanent HCT-8 [HRT-18] (ATCC-CCL-244, LGC Standards) were maintained at 37°C and 5% CO_2 using sterile RPMI 1640 (Roswell Park Memorial Institute Medium, ATCC-30-2001) supplemented with 0.3 $g.l^{-1}$ L-glutamine (Sigma-Aldrich, Darmstadt, Germany), 10% horse serum (ATCC-30-2021), 100 UI penicillin, and streptomycin 0.1 $mg.ml^{-1}$ (Sigma-Aldrich). Madine-Darby canine kidney – MDCK (ATCC- CCL-34™) cell line was kindly provided by Dr. Cyril Barbesange, National Reference Center for Influenza, Sciensano, Belgium. Cells were grown in DMEM (Gibco) containing 5 % fetal bovine serum (FBS) (Gibco), 3.7 $mg.ml^{-1}$ sodium bicarbonate, 10 µM HEPES buffer (AppliChem GmbH, Darmstadt, Germany), 100 $U.ml^{-1}$ Penicillin, 100 $\mu g.ml^{-1}$ Streptomycin. Both cell lines were seeded at a density of 2.5x105/ml at 37°C in a 5% CO_2 incubator Thermo Forma 310 (Thermo Fisher Scientific, MA, USA), in 96-well plates (Corning® Costar®, USA), 25 $\mu g.ml^{-1}$ Amphotericin B for 24 hours until monolayer confluency is reached.

Viruses

Human coronavirus OC-43 (HCoV-OC43) (ATCC: VR-1558) strain was propagated in HCT-8 cells in a maintenance solution of RPMI 1640, supplemented with 2% horse serum, 100 U/ml penicillin, and 100 $\mu g.ml^{-1}$ Streptomycin. A total of 5 days after infection, the cells were lysed by 2 freeze and thaw cycles, and the virus was titrated according to the Reed and Muench formula [47]. The infectious titer of the stock virus was $10^{6.0}$ cell culture infectious doses 50% in 1 ml ($CCID50.ml^{-1}$).

Allantoic fluid and MDCK-derived seasonal influenza A virus (IAV) strain A/Panama/07/99 (H3N2) (National Center for Infectious and Parasitic Diseases - NCIPD, Sofia, Bulgaria) were used. The infectious titer of the stock virus was $T=10^{-5,0}$ lg $CCID50.ml^{-1}$ and used as a stock suspension or at a working dose of 100 $CCID50\ ml^{-1}$.

Cytotoxicity assay

Cytotoxicity at the 72nd hour on HCT-8 and MDCK cells was evaluated first by visual microscopic observation and then by cell viability assessment after treatment with varying

 doi:10.20944/preprints202404.1537.v1

concentrations of test samples following neutral red (NR) dye uptake assay as described previously [46]. As a reference antiviral inhibitor of coronavirus replication, the stock solution of Veklury® (Gilead Science Inc. Ireland UC) with a concentration of 150 mg.ml^{-1} was used; it was prepared in double distilled water and the concentration of remdesivir (REM) in the stock solution was estimated of 8.3 x 10^{-3} M. As a reference antiviral inhibitor of influenza virus replication, oseltamivir phosphate (OS) (Hoffman-LaRoche, Switzerland) was used.

Antiviral activity assay

The cells were cultivated in 96-well plates. After the formation of a confluent monolayer, the cells were infected with 0.1 ml viral suspension in tenfold falling dilutions. After 1 hour of adsorption, the non-adsorbed virus was removed and 0.1 ml/well maintenance medium was added to the cells. The plates were incubated at 33°C for 5 days for HCoV-OC43 and at 37°C for 3 days in 5% CO_2 atmosphere for IAV. Unintended cells were used as control, cultivated under the same conditions (cells infected with the maximum concentration of the virus demonstrating the maximum cytopathic effect). The infectious viral titer was determined by microscopic monitoring of the cellular monolayer. The visually defined cytopathic effect (CPE) was confirmed by NR Uptake Assay [19]. The optical density (OD) of each well was reported at 540 nm in a microplate reader.

A CPE inhibition test was used for assessment of the antiviral activity of the test formulation. A confluent cell monolayer in 96-well plates was infected with a 100 cell culture infectious dose of 50% (CCID50) in 0.1 ml (containing a different virus strain). After 60 min for IAV or 120 min for HCov-OC-43 of virus adsorption, the non-adsorbed virus was removed and the test formulation was added in various concentrations; the cells were incubated for 48 h at 37 °C and 5% CO_2 for IAV, or 120 h at 33 °C and 5% CO_2 for the HCov-OC-43 strain. The CPE was determined using a neutral red uptake assay, and the percentage of CPE inhibition for each concentration of the test sample was calculated according to a protocol described previously [19]. The 50% inhibitory concentration (IC_{50}) was defined as the concentration of the test substance that inhibited 50% of viral replication when compared to the virus control.

Virucidal Assay

Samples of 1 ml containing virus (10^5 CCID50) and test formulation in its maximum tolerated concentration (MTC) were combined in a 1:1 ratio and subsequently stored at room temperature for different time intervals (15, 30, 45, and 60 min). Then, the residual infectious virus content in each sample was determined by the end-point dilution method, and Δlgs compared to the untreated controls were evaluated.

Statistical analysis

Data were recorded using Gen5® and further processed by Excel® Microsoft. The values of CC_{50} were calculated using non-linear regression analysis (GraphPad Software, San Diego, California, USA). The values were presented as means ± SD from three independent experiments.

Author Contributions: Conceptualization, N.I.; methodology, N.I, N.E., L.S., N.V-I., K.B., G.S.; software, N.I.; validation, V.A., N.E., K.B, and L.S; formal analysis, N.I., N.E., and L.S; investigation, N.I., K.B; resources, N.I.; data curation, N.I, L.S.; writing—original draft preparation, N.I., L.S, and K.B; writing—review and editing, V.A.; visualization, N.I.; supervision, V.A.; project administration, N.I., V.A.; funding acquisition, V.A. All authors have read and agreed to the published version of the manuscript.

Funding: This research was funded by the Medical University of Varna, Bulgaria.

Acknowledgments: We would like to express our gratefulness to the National program "Young scientists and post-doctoral researchers-2", Bulgaria.

Conflicts of Interest: The authors declare no conflicts of interest. The funders had no role in the design of the study; in the collection, analyses, or interpretation of data; in the writing of the manuscript; or in the decision to publish the results.

References

 doi:10.20944/preprints202404.1537.v1

1. Vigani: B.; Rossi, S.; Sandri, G.; Bonferoni, M.C.; Caramella, C.M.; Ferrari, F. Recent Advances in the Development of In Situ Gelling Drug Delivery Systems for Non-Parenteral Administration Routes. *Pharmaceutics* **2020**, *12*, 859. https://doi.org/10.3390/pharmaceutics12090859
2. Brambilla, E.; Locarno, S.; Gallo, S.; Orsini, F.; Pini, C.; Farronato, M.; Thomaz, D.V.; Lenardi, C.; Piazzoni, M.; Tartaglia, G. Poloxamer-Based Hydrogel as Drug Delivery System: How Polymeric Excipients Influence the Chemical-Physical Properties. *Polymers* **2022**, *14*, 3624. https://doi.org/10.3390/polym14173624
3. Madan, M.; Bajaj, A.; Lewis, S.; Udupa, N.; Baig, J.A. In situ forming polymeric drug delivery systems. *Indian J Pharm Sci.* **2009**, *71*, 242-51. https://doi.org/10.4103/0250-474X.56015
4. Perkuši´c, M.; Niži´c Nodilo, L.; Ugrina, I.; Špoljari´c, D.; Jakobuši´c Brala, C.; Pepi´c, I.; Lovri´c, J.; Safundži´c Ku˘cuk, M.; Trenkel, M.; Scherließ, R.; et al. Chitosan-Based Thermogelling System for Nose-to-Brain Donepezil Delivery: Optimising Formul tion Properties and Nasal Deposition Profile. *Pharmaceutics* **2023**, *15*, 1660. https://doi.org/10.3390/pharmaceutics15061660
5. Suhagiya, K.; Borkhataria, C. H.; Gohil, S.; Manek, R. A.; Patel, K. A.; Patel, N. K.; Patel, D. V. Development of mucoadhesive in-situ nasal gel formulation for enhanced bioavailability and efficacy of rizatriptan in migraine treatment. *Results in Chemistry* **2023**, *6*, 101010. https://doi.org/10.1016/j.rechem.2023.101010
6. Riaz, M.; Zaman, M.; Hameed, H.; Sarwar, H.S.; Khan, M.A.; Irfan, A.; Shazly, G.A.; Paiva-Santos, A.C.; Jardan, Y.A.B. Lamotrigine-Loaded Poloxamer-Based Thermo-Responsive Sol–Gel: Formulation, In Vitro Assessment, Ex Vivo Permeation, and Toxicology Study. *Gels* **2023**, *9*, 817. https://doi.org/10.3390/gels9100817
7. Williamson, S.; Dennison, L.; Greenwell, K.; Denison-Day, J.; Mowbray, F.; Richards-Hall, S.; Smith, D.; Bradbury, K.; Ainsworth, B.; Little, P.; Geraghty, A. W. A.; Yardley, L. Using nasal sprays to prevent respiratory tract infections: a qualitative study of online consumer reviews and primary care patient interviews. *BMJ Open* **2022**, *12*, e059661. https://doi.org/10.1136/bmjopen-2021-059661
8. Alsaqqa, H. H. Building the Culture of Public Health as a Positive Reflection from the COVID-19 Crisis. *Risk Management and Healthcare Policy* **2022**, *15*, 1683–1693. https://doi.org/10.2147/rmhp.s365233
9. Ivanova, N.; Sotirova, Y.; Gavrailov, G.; Nikolova, K.; Andonova, V. Advances in the Prophylaxis of Respiratory Infections by the Nasal and the Oromucosal Route: Relevance to the Fight with the SARS-CoV-2 Pandemic. *Pharmaceutics* **2022**, *14*, 530. https://doi.org/10.3390/pharmaceutics14030530
10. Bellotti, D.; D'Accolti, M.; Pula, W.; Huang, N.; Simeliere, F.; Caselli, E.; Esposito, E.; Remelli, M. Calcitermin-Loaded Smart Gels Activity against *Candida albicans*: A Preliminary In Vitro Study. *Gels* **2023**, *9*, 165. https://doi.org/10.3390/gels9020165
11. Cook, M. T.; Haddow, P.; Kirton, S. B.; McAuley, W. J. Polymers Exhibiting Lower Critical Solution Temperatures as a Route to Thermoreversible Gelators for Healthcare. *Advanced Functional Materials* **2020,** *31*. 2008123. https://doi.org/10.1002/adfm.202008123
12. Djabourov, M. Gels. In *NMR and MRI of Gels*; Editor Deene, Y.D.; Royal Society of Chemistry: London, United Kingdom, 2020; pp.1–44. https://doi.org/10.1039/9781788013178-00001
13. Russo, E.; Villa, C. Poloxamer Hydrogels for Biomedical Applications. *Pharmaceutics* **2019**, *11*, 671. https://doi.org/10.3390/pharmaceutics11120671
14. da Silva, J. B.; Cook, M. T.; Bruschi, M. L. Thermoresponsive systems composed of poloxamer 407 and HPMC or NaCMC: mechanical, rheological and sol-gel transition analysis. *Carbohydrate Polymers* **2020**, *240*, 116268. https://doi.org/10.1016/j.carbpol.2020.116268
15. Pagano, C.; Giovagnoli, S.; Perioli, L.; Tiralti, M. C.; Ricci, M. Development and characterization of mucoadhesive-thermoresponsive gels for the treatment of oral mucosa diseases. *European Journal of Pharmaceutical Sciences* **2020,** *142*, 105125. https://doi.org/10.1016/j.ejps.2019.105125
16. Perez-Robles, S.; Carotenuto, C.; Minale, M. HPMC Hydrogel Formation Mechanisms Unveiled by the Evaluation of the Activation Energy. *Polymers* **2022**, *14*, 635. https://doi.org/10.3390/polym14030635
17. Joshi, S.C. Sol-Gel Behavior of Hydroxypropyl Methylcellulose (HPMC) in Ionic Media Including Drug Release. *Materials* **2011**, *4*, 1861-1905. https://doi.org/10.3390/ma4101861
18. Abla, K.K.; Domiati, S.; El Majzoub, R.; Mehanna, M.M. Propranolol-Loaded Limonene-Based Microemulsion Thermo-Responsive Mucoadhesive Nasal Nanogel: Design, In Vitro Assessment, Ex Vivo Permeation, and Brain Biodistribution. *Gels* **2023**, *9*, 491. https://doi.org/10.3390/gels9060491
19. Ivanova, N.; Ermenlieva, N.; Simeonova, L.; Kolev, I.; Slavov, I.; Karashanova, D.; Andonova, V. Chlorhexidine–Silver Nanoparticle Conjugation Leading to Antimicrobial Synergism but Enhanced Cytotoxicity. *Pharmaceutics* **2023**, *15*, 2298. https://doi.org/10.3390/pharmaceutics15092298
20. Francisco, P.; Neves Amaral, M.; Neves, A.; Ferreira-Gonçalves, T.; Viana, A.S.; Catarino, J.; Faísca, P.; Simões, S.; Perdigão, J.; Charmier, A.J.; et al. Pluronic® F127 Hydrogel Containing Silver Nanoparticles in Skin Burn Regeneration: An Experimental Approach from Fundamental to Translational Research. *Gels* **2023**, *9*, 200. https://doi.org/10.3390/gels9030200
21. Liu, T.; Aman, A.; Ainiwaer, M.; Ding, L.; Zhang, F.; Hu, Q.; Song, Y.; Ni, Y.; Tang, X. Evaluation of the anti-biofilm effect of poloxamer-based thermoreversible gel of silver nanoparticles as a potential medication for root canal therapy. *Scientific Reports* **2021,** *11*, 12577. https://doi.org/10.1038/s41598-021-92081-7

22. Wunnoo, S.; Bilhman, S.; Waen-ngoen, T.; Yawaraya, S.; Paosen, S.; Lethongkam, S.; Kaewnopparat, N.; Voravuthikunchai, S. P. Thermosensitive hydrogel loaded with biosynthesized silver nanoparticles using Eucalyptus camaldulensis leaf extract as an alternative treatment for microbial biofilms and persistent cells in tissue infections. *Journal of Drug Delivery Science and Technology* **2022,** *74*, 103588. https://doi.org/10.1016/j.jddst.2022.103588
23. Wunnoo, S.; Lorenzo-Leal, A. C.; Voravuthikunchai, S. P.; Bach, H. Advanced biomaterial agent from chitosan/poloxamer 407-based thermosensitive hydrogen containing biosynthesized silver nanoparticles using Eucalyptus camaldulensis leaf extract. *PLOS One* **2023**, *18*, e0291505. https://doi.org/10.1371/journal.pone.0291505
24. Bates, M. G.; Risselada, M.; Peña-Hernandez, D. C.; Hendrix, K.; Moore, G. E. Antibacterial activity of silver nanoparticles against Escherichia coli and methicillin-resistant Staphylococcus pseudintermedius is affected by incorporation into carriers for sustained release. *American Journal of Veterinary Research* **2024**, *85*, 1–11. https://doi.org/10.2460/ajvr.23.10.0229
25. Salem, H. F.; Nafady, M. M.; Ewees, M. G. E.-D.;Hassan, H.; Khallaf, R. A. Rosuvastatin calcium-based novel nanocubic vesicles capped with silver nanoparticles-loaded hydrogel for wound healing management: optimization employing Box–Behnken design:in vitroandin vivoassessment. *Journal of Liposome Research* **2021**, *32*, 45–61. https://doi.org/10.1080/08982104.2020.1867166
26. Chen, L.-C.; Lin, S.-Y.; Cheng, W.-J.; Sheu, M.-T.; Chung, C.-Y.; Hsu, C.-H.; Lin, H.-L. Poloxamer sols endowed with in-situ gelability and mucoadhesion by adding hypromellose and hyaluronan for prolonging corneal retention and drug delivery. *Drug Delivery* **2023**, *30*, 2158964. https://doi.org/10.1080/10717544.2022.2158964
27. Fakhari, A.; Corcoran, M.; Schwarz, A. Thermogelling properties of purified poloxamer 407. *Heliyon* **2017,** *3*, e00390. https://doi.org/10.1016/j.heliyon.2017.e00390
28. Tatarchuk, V. V.; Bulavchenko, A. I.; Druzhinina, I. A. Kinetics of dissolution of silver nanoparticles inside triton N-42 reversed micelles. *Russian Journal of Inorganic Chemistry* **2009**, 54, 1678–1683. https://doi.org/10.1134/s0036023609100295
29. Huang, F.; Gao, Y.; Zhang, Y.; Cheng, T.; Ou, H.; Yang, L.; Liu, J.; Shi, L.; Liu, J. Silver-Decorated Polymeric Micelles Combined with Curcumin for Enhanced Antibacterial Activity. *ACS Appl. Mater. Interfaces* **2017**, *9*, 16880–16889 https://doi.org/10.1021/acsami.7b03347
30. Ko, Y.-B.; Park, Y.-H.; MubarakAli, D.; Lee, S.-Y.; Kim, J.-W. Synthesis of antibacterial hydroxypropyl methylcellulose and silver nanoparticle biocomposites via solution plasma using silver electrodes. *Carbohydrate Polymers* **2023**, 302, 120341. https://doi.org/10.1016/j.carbpol.2022.120341
31. Williams, G.; Suman, J. D. In Vitro Anatomical Models for Nasal Drug Delivery. *Pharmaceutics* **2022**, *14*, 1353. https://doi.org/10.3390/pharmaceutics14071353
32. Du, J.; Shao, X.; Bouteiller, J-M.C.; Lu, A.; Asante, I.; Louie, S.; Humayun, M. S.; Lazzi, G. Computational optimization of delivery parameters to guide the development of targeted Nasal spray. *Sci Rep* **2023,** *13*, 4099. https://doi.org/10.1038/s41598-023-30252-4
33. Beule, A.G. Physiology and pathophysiology of respiratory mucosa of the nose and the paranasal sinuses. *GMS Curr Top Otorhinolaryngol Head Neck Surg.* **2010**, *9*, 1-24. https://doi.org/10.3205/cto000071
34. Leal, J.; Smyth, H. D. C.; Ghosh, D. Physicochemical properties of mucus and their impact on transmucosal drug delivery. *International Journal of Pharmaceutics* **2017**, *532*, 555–572. https://doi.org/10.1016/j.ijpharm.2017.09.018
35. Pernakov, M.; Ermini, M. L.; Sulaieva, O.; Cassano, D.; Santucci, M.; Husak, Y.; Korniienko, V.; Giannone, G.; Yusupova, A.; Liubchak, I.; Hristova, M. T.; Savchenko, A.; Holubnycha, V.; Voliani, V.; Pogorielov, M. Complementary Effect of Non-Persistent Silver Nano-Architectures and Chlorhexidine on Infected Wound Healing. *Biomedicines* **2021**, *9*, 1215. https://doi.org/10.3390/biomedicines9091215
36. Jones-Nelson, O.; Hilliard, J. J.; DiGiandomenico, A.; Warrener, P.; Alfaro, A.; Cheng, L.; Stover, C. K.; Cohen, T. S.; Sellman, B. R. The Neutrophilic Response to Pseudomonas Damages the Airway Barrier, Promoting Infection by Klebsiella pneumoniae. *American Journal of Respiratory Cell and Molecular Biology* **2018**, *59*, 745–756. https://doi.org/10.1165/rcmb.2018-0107oc
37. Riquelme, S. A.; Ahn, D.; Prince, A. Pseudomonas aeruginosa and Klebsiella pneumoniae Adaptation to Innate Immune Clearance Mechanisms in the Lung. *Journal of Innate Immunity* **2018**, 10, 442–454. https://doi.org/10.1159/000487515
38. Binder, L.; Mazál, J.; Petz, R.; Klang, V.; Valenta, C. The role of viscosity on skin penetration from cellulose ether-based hydrogels. *Skin Research and Technology* **2019**, *25*, 725–734. https://doi.org/10.1111/srt.12709
39. Ivanova, N.; Andonova, V.; Jelev, I.; Dimova, G. Synthesis of silver nanoparticles with green tea-extracted reductants: a preliminary study for optimization of the preparation technique. *Scripta Scientifica Pharmaceutica* **2021**, *8*, 17-26. http://dx.doi.org/10.14748/ssp.v8i2.8453
40. Liu, Y.; Dai, C.; Wang, K.; Zhao, M.; Zhao, G.; Yang, S.; Yan, Z.; You, Q. New insights into the hydroquinone (HQ)–hexamethylenetetramine (HMTA) gel system for water shut-off treatment in high temperature

 doi:10.20944/preprints202404.1537.v1

reservoirs. *Journal of Industrial and Engineering Chemistry* **2016**, *35*, 20–28. https://doi.org/10.1016/j.jiec.2015.09.032

41. Lahrech, Kh.; Safouane, A.; Peyrellasse, J. Sol state formation and melting of agar gels rheological study. *Physica A: Statistical Mechanics and Its Applications* **2005**, *358*, 205–211. https://doi.org/10.1016/j.physa.2005.06.022
42. Zhao, J.; An, X.; Qiao, S. The extraction effect of CO2 injection on the flow properties of crude oil. *Petroleum Science and Technology* **2019**, *37*, 710–717. https://doi.org/10.1080/10916466.2018.1564769
43. Sotirova, Y.; Gugleva, V.; Stoeva, S.; Kolev, I.; Nikolova, R.; Marudova, M.; Nikolova, K.; Kiselova-Kaneva, Y.; Hristova, M.; Andonova, V. Bigel Formulations of Nanoencapsulated St. John's Wort Extract—An Approach for Enhanced Wound Healing. *Gels* **2023**, *9*, 360. https://doi.org/10.3390/gels9050360
44. Wadell, C.; Björk, E.; Camber, O. Nasal drug delivery – evaluation of an in vitro model using porcine nasal mucosa. *European Journal of Pharmaceutical Sciences* **1999,** 7, 197–206. https://doi.org/10.1016/s0928-0987(98)00023-2
45. European Directorate for the Quality of Medicines & HealthCare of the Council of Europe (EDQM). European Pharmacopoeia. Strasbourg: Council of Europe, 10.0(1), 2019; pp. 3790 – 3791
46. Repetto, G.; del Peso, A.; Zurita, J.L. Neutral red uptake assay for the estimation of cell viability/cytotoxicity. *Nat. Protoc.* **2008**, *3*, 1125–1131. https://doi.org/10.1038/nprot.2008.75
47. Reed, LJ.; Muench, H.A. Simple method of estimating fifty percent endpoints. *Am. J. Hyg*. **1938**, 27, 493–497.